Available online at www.sciencedirect.com
ScienceDirect
Journal of Solid State Chemistry 180 (2007) 2723–2733
JOURNAL OF SOLID STATE CHEMISTRY
www.elsevier.com/locate/jssc

Coupled In/Te and Ni/vacancy ordering and the modulated crystal structure of a *B*8 type, $Ni_{3\pm x}In_{1-y}Te_{2+y}$ solid solution phase

A.-K. Larsson[a,*], L. Noren[a], R.L. Withers[a], H. Rundlöf[b]

[a]*Research School of Chemistry, Australian National University, Science Road, Canberra, ACT 0200, Australia*
[b]*Inst. Materialkemi, Ångströmlaboratoriet, Box 538, S-752 21 Uppsala, Sweden*

Received 24 April 2007; received in revised form 11 July 2007; accepted 15 July 2007
Available online 9 August 2007

Abstract

The commensurate superstructures of a *NiAs/Ni₂In* type parent structure, $Ni_{3.32}InTe_2$ and $Ni_{3.12}In_{0.86}Te_{2.14}$ ($\mathbf{q} = \gamma[0\,0\,1]^*$, $\gamma = 2/3$) as well as one dimensionally incommensurate structure of Ni_3InTe_2 ($\gamma = 0.71$) were refined from neutron powder diffraction data ($R_{wp} = 4.77\%$, 4.53% and 4.91% for the three structures, respectively, at 298 K). The commensurate structures were refined in the $P6_3/mmc$ space group ($\mathbf{c} = 3\mathbf{c}_{NiAs}$). The stacking sequence at the hcp array is -In/Te/Te/- and the trigonal bipyramidal site within the In layer, Ni(2), is partially occupied while it is empty in the Te layers. The octahedral position in between the In and Te layers, Ni(1*a*), is fully occupied while the octahedral position in between two adjacent Te layers, Ni(1*b*), is partially occupied. With decreasing In and Ni content, the modulation wave vector, γ, was found to increase continuously until $\gamma = 1$. From this, crenel functions to describe the whole homogeneity range of the solid solution were constructed with the length of the atomic domains $\Delta^{Te} = \gamma$ (and hence $\Delta^{In} = \Delta^{Ni} = 1-\gamma$) and $\Delta^{Ni(1b)} = \gamma/2$ (and hence $\Delta^{Ni(1a)} = 1-\gamma/2$) which were then used for the refinement of the incommensurate structure of Ni_3InTe_2. The corresponding effect in real space is that the *single* In layers separating *double layers of Te* occur less frequent when γ in increasing until at $\gamma = 1$ the CdI_2 type structure of $Ni_{1+x}Te_2$ is reached.

Keywords: Nias type structure; Nickel telluride; Nickel indium; Neutron diffraction; Superstructure

1. Introduction

Many $T_{1\pm x}B$ phases adopt either the trigonal ($P\bar{3}m1$) CdI_2 or the hexagonal ($P6_3/mmc$) NiAs or Ni_2In average structure types (see Fig. 1) and can often exist over a wide solid solution field [1,2]. Such materials are known as *B*8 type phases. *T* is normally a transition metal atom and *B* an element from groups III–VII [1–3]. The *B* atoms in Wyckoff position 2*c* (1/3, 2/3, 1/4) form an essentially hexagonal close packed (hcp) array while the *T* atoms occupy octahedral sites therein at Wyckoff position 2*a* (0, 0, 0), giving rise to the ideal *NiAs* structure type, as shown in Fig. 1a.

In the case of transition metal-rich compounds $T_{1+x}B$, the *T* atoms also occupy a trigonal bipyramidal 2*d* site (1/3, 2/3, 3/4) within the hcp array of *B* atoms (see the dark balls in Fig. 1b). The structure type is then referred to as *Ni₂In*. In the case of transition metal poor compounds $T_{1-x}B$, the 2*d* trigonal bipyramidal sites are empty, while the transition metal atoms necessarily missing from the octahedral 2*a* sites are often not removed at random but rather selectively removed from alternate octahedral transition metal layers along **c**, thereby lowering the overall space group symmetry to $P\bar{3}m1$ (see Fig. 1c). At the extreme end of this $T_{1-x}B$ compositional range is the ideal *CdI₂* structure type, in which the octahedral transition metal layers of the *NiAs* structure type are alternately completely empty and fully occupied.

Routine investigations of many such $T_{1\pm x}B$ phases report wide range solid solution fields. More careful diffraction studies, in particular with electron diffraction methods, however, usually reveal extra satellite reflections and/or localized diffuse scattering (in addition to the Bragg reflections of the underlying $P6_3/mmc$ or $P\bar{3}m1$ average structures) suggesting additional ordering, at least on the

*Corresponding author. Fax: +61 2 6125 4692.
E-mail address: ankie.larsson@anu.edu.au (A.-K. Larsson).

0022-4596/$ - see front matter © 2007 Elsevier Inc. All rights reserved.
doi:10.1016/j.jssc.2007.07.020

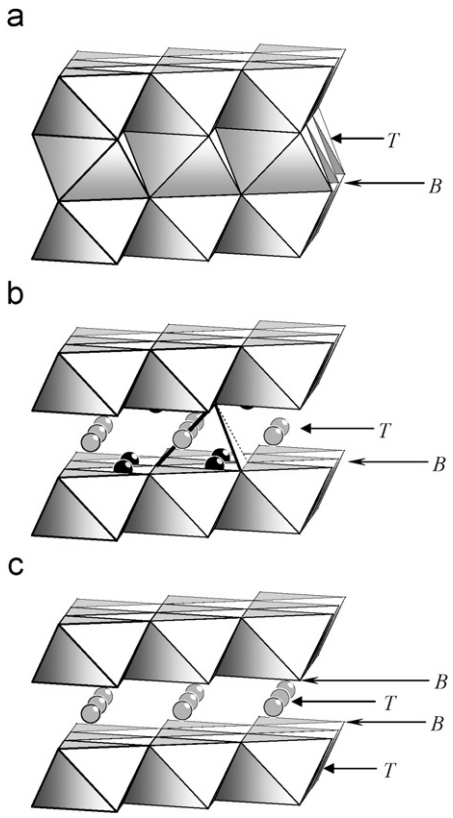

Fig. 1. Schematic representations close to the ⟨1 0 0⟩ orientation of (a) the NiAs structure type, (b) the Ni_2In structure type and (c) the CdI_2 structure type. The *B* atoms at the vertexes of the octahedra form a hexagonally close packed array in each case. In the NiAs structure type (a) and the Ni_2In structure type (b), the *T* atoms (indicated with grey spheres or in the centre of octahedra) occupy all the octahedral sites (b). In the case of the Ni_2In structure type (b), the trigonal bipyramidal site within the hcp *B* atom array is also occupied (black spheres). In the CdI_2 structure type (c), only alternate octahedral layers along *c* are fully occupied which lowers the symmetry to $P\bar{3}m1$.

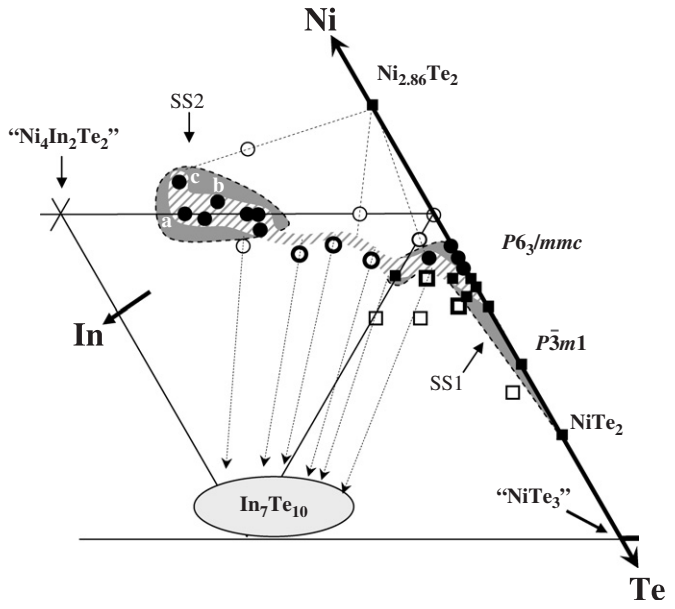

Fig. 2. A portion of the ternary Ni–Te–In phase diagram partially adapted from [7]. Single-phase samples are in filled symbols while symbols with bold outline contain minute impurities. The square symbols indicate that the 001 reflection is visible (i.e. a CdI_2 type structure) while circles indicate that this reflection is not observed (i.e. a $NiAs/Ni_2In$ type parent structure). A tentative solid solution range replacing the previously suggested SS1 and SS2 fields is given in the hatched area.

local scale [4–6]. To gain insight into the crystal chemistry underlying such ordering phenomena and controlling the composition range of such phases, it is informative to study more complex compositions such as those accessible in ternary phase diagrams—in particular those for which extensive solid solutions fields occur in the limiting binary phase diagrams such as is the case for both the Ni–In [4,5] and Ni–Te [6] binary systems. In this contribution, we report crystal structures at three compositions within a *B*8 type, $T_{1\pm x}B$ solid solution phase recently identified in the Ni–In–Te ternary system [7] (see Fig. 2) and discuss the crystal chemistry underlying the existence of this wide range non-stoichiometric solid solution phase.

In earlier work on this system [7], a solid solution field of $NiAs/Ni_2In$ average structure type with composition close to $Ni_{2.91}In_{0.8}Te_2$ (labelled SS2) was reported (see Fig. 2) and its reciprocal space carefully investigated via electron diffraction. In addition to the strong Bragg reflections of the underlying $P6_3/mmc$, $NiAs/Ni_2In$ type average structure, composition-dependent satellite reflections along $\mathbf{c}^*$ were observed (see e.g. Fig. 3a(i) and (ii)). The composition-dependent magnitude, γ, of the primary modulation wave vector associated with these satellite reflections, $\mathbf{q} = \gamma\mathbf{c}^*$, was carefully measured for the seven samples synthesized within the SS2 phase field and found to take values ranging from a minimum of 2/3 up to ~0.74 [7].

For each composition, γ was found to be relatively close to Te/(In + Te). It was thus proposed [7] that the ordering/interleaving of Te-rich and In-rich, *B* type layers (with a relative concentration of γ: $1-\gamma$) along the *c* direction had to be responsible for the observed magnitude of γ, although there could clearly be no direct one-to-one correspondence between γ and the exact In/Te ratio. The latter was attributed to a limited solubility of Te in the In layers and vice versa. It was further suggested that partially occupying trigonal bipyramidal Ni sites within the In-rich layers would increase their naturally smaller in-plane cell dimension and be the mechanism used to match the in-plane cell dimensions of the In-rich and Te-rich layers [7]. Such an ordering scheme implies that the (trigonal bipyramidal) Ni content should necessarily reduce as γ increases, i.e. as the concentration of In-rich layers decreases. Plotting the total Ni content against the observed modulation wave vector magnitude γ (see Fig. 3b), there is indeed a clear trend that the Ni content systematically decreases as γ increases.

By adding several points corresponding to high y, close to end-member, compositions of the $Ni_{1+y}Te_2$, $0 \leqslant y \leqslant \sim 0.65$, phase of CdI_2 structure type (with $\gamma = 1$, see Fig. 3a(vii)) from the SS1 type phase field onto the same plot, it becomes apparent that the SS1 phase also fits onto the same trend curve. (The binary $Ni_{1+y}Te_2$, $0 \leqslant y \leqslant 0.83$,

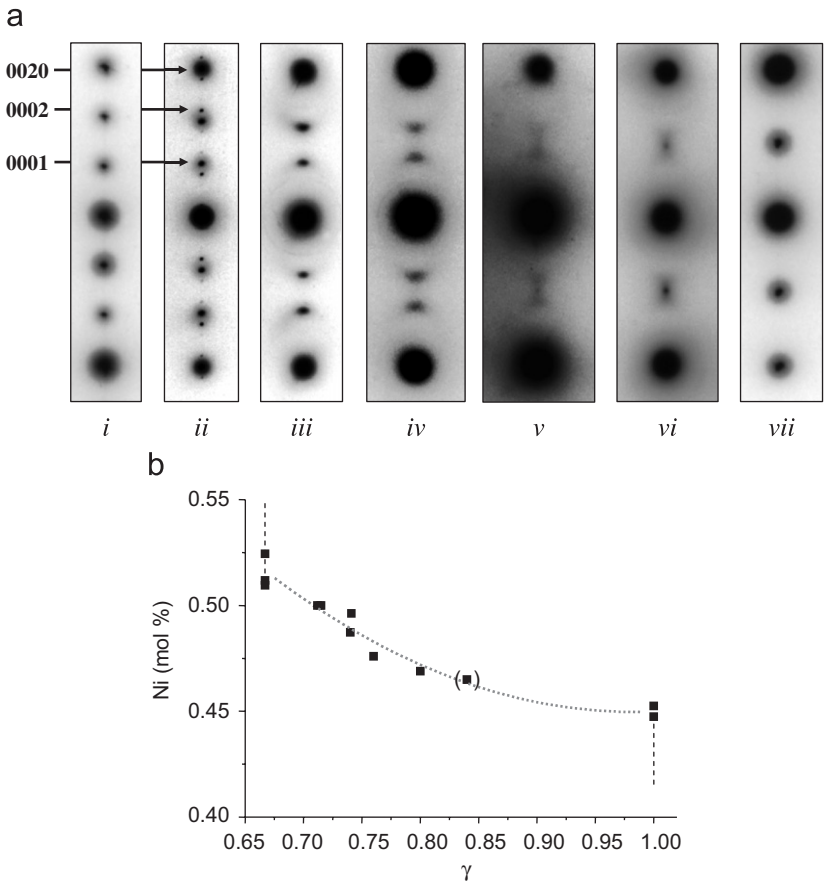

Fig. 3. (a) The central $\langle 0\,0\,l\rangle^*$ systematic row portion of $\langle \bar{1}\,1\,0\rangle$ zone axis EDP's of (i) $Ni_{3.12}In_{0.86}Te_{2.14}$ ($\gamma = 2/3$), (ii) Ni_3InTe_2 ($\gamma = 0.71$), (iii) $Ni_{2.74}In_{0.80}Te_{2.20}$ ($\gamma = 0.76$), (iv) $Ni_{2.73}In_{0.46}Te_{2.54}$ ($\gamma = 0.80$), (v) $Ni_{2.61}In_{0.34}Te_{2.66}$, (vi) $Ni_{2.63}In_{0.11}Te_{2.89}$ and (vii) $Ni_{1.50}Te_2$ ($\gamma = 1$). (i) and (ii) are from the previously reported SS2 phase field, (vi) and (vii) are from the (previously reported as) separate SS1 phase field while (iii), (iv) and (v) are from samples on a line in the phase diagram connecting these two phase field. These graduate changes from (i) to (vii) support the hypothesis there is a continuous phase field connecting the SS2 and SS1 phase fields. (b) The total nickel content of the compounds drawn as a function of the modulation wave vector, γ.

*B*8 type composition range has *P*-3*m*1, CdI_2 structure type for $0 \leqslant y \leqslant 0.65$ [8] but changes to the $P6_3/mmc$, *NiAs* structure type for $0.65 \leqslant y \leqslant 0.83$ [9]. Note that the CdI_2 structure type can be described as a $\mathbf{q} = 1\mathbf{c}^*$ (i.e. $\gamma = 1$) modulated *NiAs* structure type, see also Fig. 3a.) From this, it is hypothesized that there may indeed be a continuous solid solution pathway connecting the previously reported as separate SS1 and SS2 phase fields—γ should then be able to increase continuously all the way from 2/3 to 1, with the concentration of In-rich layers going to zero at $\gamma = 1$ leaving a resultant $Ni_{1+y}Te_2$ composition of CdI_2 structure type (see Figs. 2 and 3).

In this contribution, crystal structure refinements of neutron powder diffraction (NPD) data are reported for three of the samples from the previous study, namely Ni_3InTe_2, $Ni_{2.91}In_{0.8}Te_2$ ($= Ni_{3.12}In_{0.86}Te_{2.14}$) and $Ni_{3.32}InTe_2$ (compositions *a*, *b* and *c* in Fig. 2; cf. Table 1 of Ref. [7]) in order to investigate the above assumptions as regards the structural origin of the observed modulation. Several additional compounds with composition in between and around the previously reported SS2 and SS1 composition fields have also been synthesized (see Fig. 2) in order to investigate the above hypothesis of an extended homogeneity range linking the two fields together. The same samples were also investigated with electron diffraction (see Fig. 3a) in order to see if additional satellite reflections were present and, if so, to confirm the trend of a systematic decrease in Ni content as γ increases.

2. Experimental

2.1. Sample preparation

The compounds for the neutron diffraction experiments were synthesized by heating the elements (99.99% purity or better) in evacuated silica tubes [7]. The starting weights were: 10.9664 g ($Ni_{3.000}In_{1.000}Te_2$), 9.8684 g ($Ni_{2.914}In_{0.800}Te_2 \equiv Ni_{3.122}In_{0.857}Te_{2.143}$) and 9.6431 g ($Ni_{3.316}In_{1.000}Te_{2.000}$). The samples were initially heated at 1000 °C for 1 h. As the molten compounds wet the glass wall, slow cooling can occasionally cause cracks in an ampoule when the compound solidifies and shrinks due to the different thermal expansion coefficients of the compounds and the glass. This was avoided by quenching the ampoules in water. The intact, quenched ampoules were checked for cracks with a Tesla coil. In all cases, the vacuum remained.

In order to make sure that the vapour phase existing at elevated temperatures did not cause any change from the nominal compositions, the still sealed ampoules were further heated at 700 °C overnight and 570 °C for at least a further 2 days in order to reintegrate any more volatile phases back into the ingots. The weight changes of the resultant products were negligible: −0.020% ($Ni_{3.316}In_{1.000}Te_2$), +0.015% ($Ni_{3.122}In_{0.857}Te_{2.143}$) and −0.016% ($Ni_{3.000}In_{1.000}Te_2$), within error for the stoichiometries stated. These resultant samples were then crushed, pressed to pellets and repeatedly re-annealed in sealed quartz ampoules at 570 °C for periods which ranged between 2 weeks and 1 month. They were then checked for phase purity and completeness of reaction. At least two such long period annealings were carried out for each sample. After such treatment, the X-ray powder diffraction patterns invariably showed single-phase samples with sharp narrow line-widths in each case.

In order to further confirm these stoichiometries and to eliminate the possibility of any compositional change of the single-phase crystalline material arising from the presence of an undetected (by XRD) amorphous phase, the samples were also quantitatively analysed via electron probe micro analysis (EPMA). A JEOL 6400 scanning electron microscope (SEM) equipped with an Oxford Instruments light element EDS detector and Link ISIS SEMquant software were used. The samples were embedded in resin and polished to a $<1\,\mu m$ finish with corundum. More than 30 spot analyses were carried out for each sample at 15 kV and 1 nA using the pure elements as calibration standards. The resultant compositions were $Ni_{2.99(2)}In_{0.99(3)}Te_{2.01(4)}$, $Ni_{3.15(2)}In_{0.88(4)}Te_{2.15(5)}$ and $Ni_{3.29(3)}In_{1.00(6)}Te_{2.01(6)}$, respectively, in agreement with the nominal starting compositions to within one standard deviation. The additional samples for the electron diffraction investigation on the variation of the modulation wave vector, γ, with composition were prepared in the same manner.

2.2. Data collection

Given the very similar X-ray scattering factors of In and Te, neutron powder diffraction was used to maximize the scattering contrast between In and Te. The data were collected on the NPD diffractometer at the R2 reactor at Neutronforskningslaboratoriet (NFL) in Studsvik, Sweden at both room temperature (295 K) and 10 K. The detector system consisted of 35 ^{3}He detectors measuring the intensity in 2θ between 4° and 139.92° in steps of 0.08°. The sample was placed in a vanadium cylinder with a diameter of 10 mm. The absorption factor μR was determined from transmission measurements at $2\theta = 0°$ and found to be 0.377 (Ni_3InTe_2), 0.327 ($Ni_{3.12}In_{0.86}Te_{2.14} \equiv Ni_{2.91}In_{0.8}Te_2$) and 0.343 ($Ni_{3.32}InTe_2$), respectively. The neutron flux was $10^6\,cm^{-2}\,s^{-1}$. The wavelength ($\lambda_{neutron}$) was given as ~1.47 Å at the source and was refined to 1.4714(4) Å using the values of the unit cell parameters obtained from room temperature powder X-ray diffraction data (XRD). This wavelength was then used as fixed for all patterns. The XRD data were collected using a Guinier–Hägg camera with Si ($\lambda = 1.5406$ Å) added as an internal standard. Electron diffraction data were obtained using a Philips EM 430 transmission electron microscope (TEM) operating at 300 kV.

3. Results

3.1. Phase analysis

The previously reported SS1 and SS2 solid solution fields [7] are marked with dark grey shading and dashed outlines in Fig. 2. In order to investigate the hypothesis that these two phase fields may be connected into the one continuous phase field, additional samples were prepared with composition close to an assumed line connecting them (see Fig. 2). All samples represented by square symbols in Fig. 2 contain the 001 Bragg reflection diagnostic of the CdI_2 structure type but forbidden by the *NiAs* structure type. In samples represented by circles, this 001 Bragg reflection is missing. Filled symbols correspond to single-phase samples while heavily outlined open symbols represent essentially single-phase samples with barely detectable trace amounts of either In_7Te_{10} or $Ni_{2.86}Te_2$. More lightly outlined open symbols represent two-phase samples with clearly detectable amounts of either In_7Te_{10} or $Ni_{2.86}Te_2$ present. These results strongly suggest the existence of a continuous but quite compositionally narrow *NiAs*/Ni_2In average structure solid solution field connecting the SS1 and SS2 solid solution fields (shown by the hatched phase field in Fig. 2).

The existence of such a continuous solid solution field is also strongly supported by the quite gradual (essentially continuous) changes in the nature of electron diffraction patterns (EDPs) with composition on moving from one side of the hatched phase field in Fig. 2 to the other. Fig. 3a, for example, shows the central $\langle 0\,0\,l \rangle^*$ systematic row portion of $\langle \bar{1}\,1\,0 \rangle$ zone axis EDP's of (i) $Ni_{3.12}In_{0.86}Te_{2.14}$ ($\gamma = 2/3$), (ii) Ni_3InTe_2 ($\gamma = 0.71$) (both within the previously reported SS2 solid solution field), (iii) $Ni_{2.74}In_{0.80}Te_{2.20}$ ($\gamma = 0.76$), (iv) $Ni_{2.73}In_{0.46}Te_{2.54}$ ($\gamma = 0.80$), (v) $Ni_{2.61}In_{0.34}Te_{2.66}$ (the three new, essentially single-phase samples falling between the previously reported SS1 and SS2 solid solution fields in Fig. 2), (vi) $Ni_{2.63}In_{0.11}Te_{2.89}$ and (vii) $Ni_{1.50}Te_2$ ($\gamma = 1$) (both within the previously reported SS1 solid solution field).

Note that the EDPs shown in Fig. 3a were quite reproducible from grain to grain and that the measured value of γ for the intermediate samples (iii) and (iv) significantly extend the previously reported range of $2/3 \leqslant \gamma \leqslant 0.74$. Finally, note that while essentially sharp satellite reflections are present for the relatively high In content samples (i)–(iv), this is no longer true for the low In content samples (v) and (vi). In the case of sample (v), the relatively sharp 0001 and 002$\bar{1}$ satellite reflections of sample (iv), for example, have been replaced by a limited

diffuse streak running from $\sim 0.85\mathbf{c}^*$ to $1.15\mathbf{c}^*$ suggesting that the long range ordering of the In-rich layers, although still present, is beginning to break down. By sample (vi), a reflection at $\mathbf{c}^*$ is beginning to emerge although some limited diffuse streaking is still apparent. Taken together, the above observations strongly support the existence of a compositionally narrow but continuous solid solution field linking the end-members with $\gamma = 2/3$ and 1, respectively.

3.2. Symmetry considerations

The relevant (3+1)-d superspace group symmetry for this SS2 solid solution phase is $P6_3/mmc(00\gamma)000$ (superspace group no. 194.1 in Table 9.8.3.5 of Ref. [10]), with $\gamma \geqslant 2/3$ (see Ref. [7]). Given the underlying $P6_3/mmc$, $B8$ type average structure (octahedral Ni(1) at 000, trigonal bipyramidal Ni(2) at $-1/3$, 1/3, $+1/4$ and (In,Te) at $-1/3$, 1/3, $-1/4$), such a superspace group symmetry allows occupational modulation on all three sites but constrains any associated displacive shifts to be only along the c direction.

When γ takes a rational value, such as e.g. 2/3, a commensurate superstructure results with the resultant 3-d space group symmetry formally dependent upon the so-called global phase, ϕ [11,12]. For the case $\gamma = 2/3$, this resultant 3-d space group symmetry is $P6_3mc$ (for a general global phase) and $P6_3/mmc$ if ϕ takes either of the values $n/3$ or $(1/6+n/3)$, n an integer. The commensurate superstructure refinements below were carried out in the latter $P6_3/mmc$ space group as no evidence requiring a lower symmetry could be detected. Given the above evidence for a continuous solid solution field connecting the previously reported SS1 and SS2 regions, it is important to also consider the other end-member limit of $\gamma = 1/1$. In this case, the resultant 3-d space group symmetry is $P\bar{3}m1$ if $\phi = 2n/4$, $P\bar{6}m2$ if $\phi = (2n+1)/4$ and $P3m1$ otherwise. $P\bar{3}m1$ corresponds to the space group symmetry of the end-member $Ni_{1+y}Te_2$, $0 \leqslant y \leqslant \sim 0.65$, solid solution of CdI_2 structure type (see Fig. 2).

3.3. Crystal structure refinements

Neutron powder diffraction data were collected for three compounds (Ni_3InTe_2, $Ni_{3.12}In_{0.86}Te_{2.14}$ and $Ni_{3.32}InTe_2$) within the SS2 solid solution field at both 10 and 295 K and refined with the program JANA2000 [13]. The magnitude of the primary modulation wave vector, γ, takes the value of 0.71 for Ni_3InTe_2. For the other two compositions, γ takes the value of 2/3 despite the similar but nonetheless distinct compositions. Although all indications are that γ varies continuously within the solid solution field, suggesting that the crystal structures at all compositions could be described as continuously variable, (3+1)-d incommensurately modulated structures, we start with conventional, commensurate superstructure refinements of $Ni_{3.12}In_{0.86}Te_{2.14}$ and $Ni_{3.32}InTe_2$. These refined structures of the $\gamma = 2/3$ end-members are then used in conjunction with the known $\gamma = 1$ end-member to model the (3+1)-d incommensurate structure of Ni_3InTe_2 and other members of the solid solution field. In all cases, after initial refinements, it was clear that preferred orientation (along 0 0 1) affected all samples. This was corrected for using the March-Dollase function. With this correction, refinement was in general straight-forward and proceeded smoothly.

3.3.1. Commensurate superstructure refinements

3.3.1.1. $Ni_{3.32}InTe_2$. The refined crystal structure of $Ni_{3.32}InTe_2$ is shown in projection down $\langle 1\,0\,0 \rangle$ in Fig. 4 while the refinement details and structural parameters are given in Tables 1–3. The final profile fit and difference plot is shown in Fig. 5. The In(1) atoms together with the Te(2) atoms form the fully occupied, hcp array of In and Te atoms with the layer stacking sequence. Te/Te/In/Te/Te/In. The Ni(1*a*) atoms fully occupy the octahedral sites in the two Ni layers directly adjacent to each In layer, the Ni(1*b*) atoms partially occupy the octahedral sites

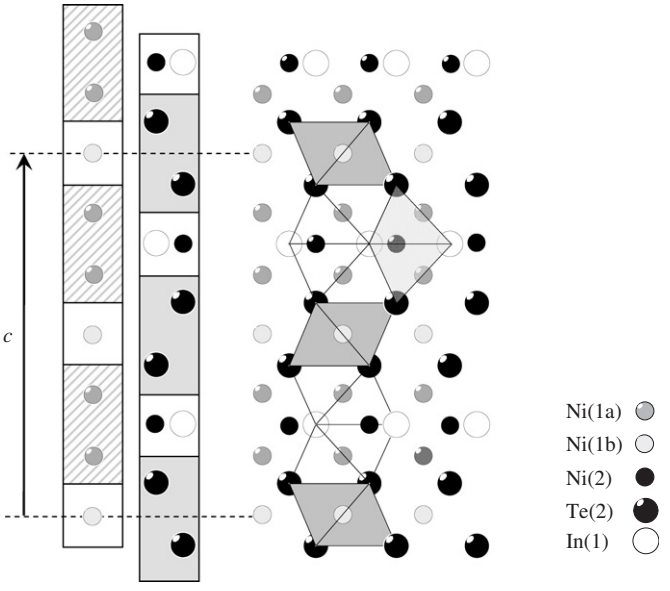

Fig. 4. The commensurate crystal structure of $Ni_{3.32}InTe_2$ along $\langle 1\,0\,0 \rangle$. To the left, the (3+1)-d description of the structure is indicated with grey and white domains along **c** representing a crenel type function with the real space repeat 3/2**c** (corresponding to 1/**q**). The width of the complementary crenel functions for Te and In are shown: $\Delta^{Te} = 2/3$ is indicated in grey while $\Delta^{In} = 1/3$ is indicated in white.

Table 1
Unit cell parameters from the superstructure refinements

	Sample			
	$Ni_{3.32}InTe_2$		$Ni_{3.12}In_{0.86}Te_{2.14}$	
	10 K	295 K	10 K	295 K
a	4.0257(2)	4.0388(2)	4.0087(1)	4.0209(2)
c	15.6828(8)	15.7321(9)	15.7213(8)	15.7749(8)
c/3*a*	1.2986	1.2984	1.3073	1.3077

Table 2
Refined parameters from the superstructure refinements

	Sample			
	$Ni_{3.32}InTe_2$		$Ni_{3.12}In_{0.86}Te_{2.14}$	
	10 K	295 K	10 K	295 K
z[Ni(1a)]	0.8366(3)	0.8368(3)	0.8363(2)	0.8361(3)
z[Te(2)]	0.4130(4)	0.4124(4)	0.4134(4)	0.4126(4)
SOF[Ni(1b)]	0.805(6)	0.809(6)	0.738(3)	0.737(6)
SOF[Ni(2)]	0.505	0.497	0.383	0.386
SOF[In(1)]	1	1	0.857	0.857
SOF[Te(1)]	0	0	0.143	0.143
U_{iso}[Ni]	0.0048(3)	0.0123(4)	0.0055(3)	0.0127(4)
U_{iso}[In(1)/Te(1)]	0.028(3)	0.035(3)	0.025(3)	0.032(3)
U_{iso}[Te(2)]	0.0046(9)	0.010(1)	0.0042(9)	0.010(1)

Ni(1a) is in Wyckoff position 4e (0 0 z); Ni(1b) in 2a (0 0 0); Ni(2) in 2c (1/3, 2/3, 1/4); In/Te(1) in 2d (1/3, 2/3, 3/4), Te(2) in 4f (1/3, 2/3, z).

between two adjacent Te layers while the Ni(2) atoms partially occupy the trigonal bipyramidal positions within each In layer. Initially, the occupancies of the Ni(1b) and Ni(2) sites were allowed to vary independently. The refined Ni content, however, always remained very close to that expected from the nominal composition. For the final refinement cycles, only one common ADP for the three Ni sites was refined and the overall Ni content was restricted to the nominal value.

The two refined z parameters, z[Ni(1a)] and z[Te(2)] (see Table 2), are perhaps more instructively re-written in the form $z[\mathrm{Ni}(1a)] = (10+\varepsilon[\mathrm{Ni}(1a)])/12$ and $z[\mathrm{Te}(2)] = (5-\varepsilon[\mathrm{Te}])/12$, respectively (cf. Fig. 4) in order to highlight the $(\varepsilon[\mathrm{Ni}(1a)]/12)c \sim 0.051$ Å and $(\varepsilon[\mathrm{Te}(2)]/12)c \sim 0.069$ Å displacive relaxations of the Ni(1a) and Te(2) layers along c away from their average structure positions induced by the In/Te and Ni/vacancy ordering.

Table 3
Refinement residuals

	Sample					
	$Ni_{3.32}InTe_2$		$Ni_{3.12}In_{0.86}Te_{2.14}$		Ni_3InTe_2	
	10 K	298 K	10 K	298 K	10 K	298 K
R_{wp}	4.81	4.77	4.87	4.53	4.82	4.91
Parameters	7	7	7	7	5	5
R_w(obs)	2.37(108 + 15)	2.40(107 + 16)	1.92(108 + 14)	2.23(109 + 13)	2.13(89 + 32)	2.88(101 + 20)
R_w(all)	2.41	2.41	1.94	2.25	2.34	2.91
R_w(obs) main					1.34(41 + 2)	2.65(41 + 2)
R_w(all) main					1.34	2.65
R_w(obs) 1st					3.07(48 + 30)	3.13(60 + 18)
R_w(all) 1st					3.45	3.20

The numbers in the parentheses refer to the number of observed + number of unobserved reflections of the type.

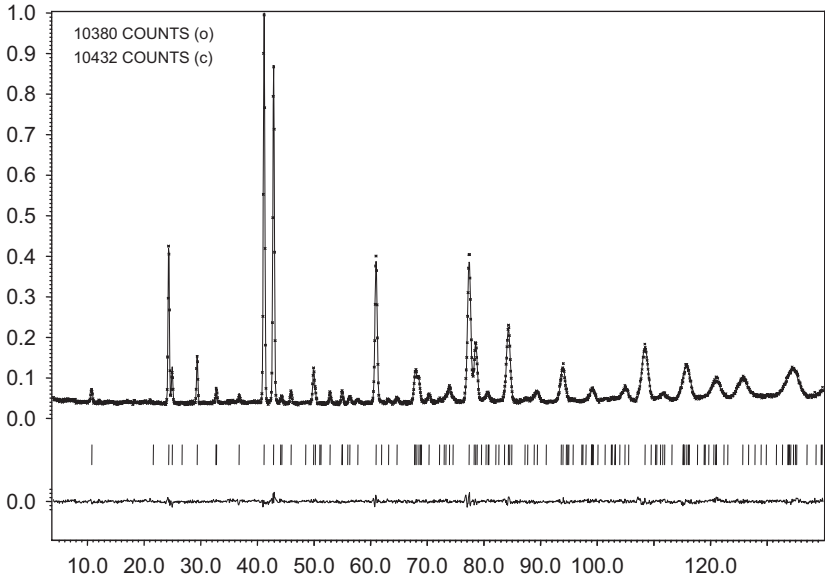

Fig. 5. The final profile fit for the sample $Ni_{3.32}InTe_2$ (at 10 K).

The Ni(2)–Te distance in the Ni(2)In_3Te_2 trigonal bipyramid surrounding each Ni(2) site (to the Te atoms at the top and bottom of the trigonal bipyramid) is 2.55 Å while the Ni(2)–In intra-layer distance within the base of the trigonal bipyramid is only 2.33 Å, quite short by comparison with all other near neighbour distances in the refined structure e.g. d(Ni(1a)–In) = 2.70 Å and d(Ni(1a)–Te) = 2.62 Å for the Ni(1a)In_3Te_3 octahedron while d(Ni(1b)–Te) = 2.71 Å for the Ni(1b)Te_6 octahedron. In order to relieve local strain, In(1) atoms might therefore be expected to locally displace away from the occupied Ni(2) positions within the Ni(2)/In(1) layers and towards neighbouring vacant Ni(2) sites. Some evidence for this can be found in the relatively large, and essentially temperature-independent, isotropic atomic displacement parameter (ADP) refined for In (see Table 2).

The overall structure can be described in terms of the regular intergrowth of a three atom layer thick, *NiAs/Ni₂In* type, layered structure (denoted by the white region on the occupancy domain bar diagram to the immediate left of the structure in Fig. 4) with a five atom layer thick, *CdI₂* type layered structure (denoted by the grey shaded region on the same bar diagram). Note that the latter five atom layer thick, building block corresponds to the structure of the $\gamma = 1$ end-member $Ni_{1+y}Te_2$ of *CdI₂* structure type [8]. Given a continuous solid solution field linking the end-members with $\gamma = 2/3$ and 1, the same two layered structural building blocks are likely to be present at any intermediate composition. The *NiAs/Ni₂In* region of the structure (with its characteristic partially filled trigonal bipyramidal positions) corresponds formally to a net composition $Ni_{1.49}In$ while the *CdI₂* region of the structure (with its characteristic fully occupied followed by partially occupied octahedral layers) corresponds formally to the net composition $Ni_{1.82}Te_2$.

3.3.1.2. $Ni_{3.12}In_{0.86}Te_{2.14}$. The superstructure refinement at the composition $Ni_{3.12}In_{0.86}Te_{2.14}$ behaved very similarly to the refinement of $Ni_{3.32}InTe_2$ described above. The only real difference was in the refined occupancies of the In(1), Ni(1b) and Ni(2) sites (see Table 2). The overall composition does not allow In and Te to be clearly separated into two unmixed sites. Assuming 100% occupancy of the octahedral Ni(1a) site, it was concluded from refinements that the Te(2) position also remained 100% occupied by Te while the 'In(1)' site necessarily must have some Te mixed onto the site. The occupancy of this In(1)/Te(1) position was thus locked to 85.7% In and 14.3% Te reflecting the overall composition of the sample.

The refined isotropic atomic displacement parameters (ADPs) both at 295 K as well as at 10 K refined to comparable values to those obtained for $Ni_{3.32}InTe_2$. The same conclusions as regards Ni(2)/vacancy ordering and associated induced in-plane In displacements are thus also valid for this composition. The somewhat lower refined occupancies of the trigonal bipyramidal Ni(2) and octahedral Ni(1a) sites are only to be expected given the lower overall Ni content for this $Ni_{3.12}In_{0.86}Te_{2.14}$ sample.

3.3.2. Incommensurate structure modelling and refinements

3.3.2.1. Incommensurate structure modelling. In order to refine the structure of a general incommensurate member of the SS2 solid solution field such as Ni_3InTe_2 (see below), it is first of all necessary to describe the coupled In/Te and Ni/vacancy occupational ordering associated with any primary modulation wave vector magnitude, γ, in terms of occupational crenel functions (see e.g. Refs. [14–16]) describing which of the average structure layers are occupied by which atom types as a function of $\bar{x}_4 = \mathbf{q}\cdot(\mathbf{r}_\mu + \mathbf{t})$, where $\mathbf{q} = \gamma\mathbf{c}^*$ and $(\mathbf{r}_\mu + \mathbf{t})$ labels the position of the μth atom in the parent unit cell labelled by the Bravais lattice vector $\mathbf{t}$. Three such occupational crenel functions are required, one for the 'In'/'Te' layers (containing 'Te' regions and 'In' regions), one for the Ni(2) trigonal bipyramidal layers (containing partially occupied Ni(2) regions and vacancy regions) and one for the Ni(1a)/Ni(1b) octahedral layers (containing fully occupied Ni(1a) regions and partially occupied Ni(1b) regions).

Given the close (but not exact) relationship between γ and Te/(In + Te), the above end-member commensurate superstructure refinements (for $\gamma = 2/3$) as well as the realization that the $Ni_{1+y}Te_2$ structure of *CdI₂* structure type must constitute the other end-member structure for $\gamma = 1$, the only possible choice for these occupational crenel functions are those shown in Fig. 6. Note that for γ to act as a "chemical ruler", i.e. to be determined by composition, the occupational domain heights (compositions) and widths within these crenel functions are necessarily strictly

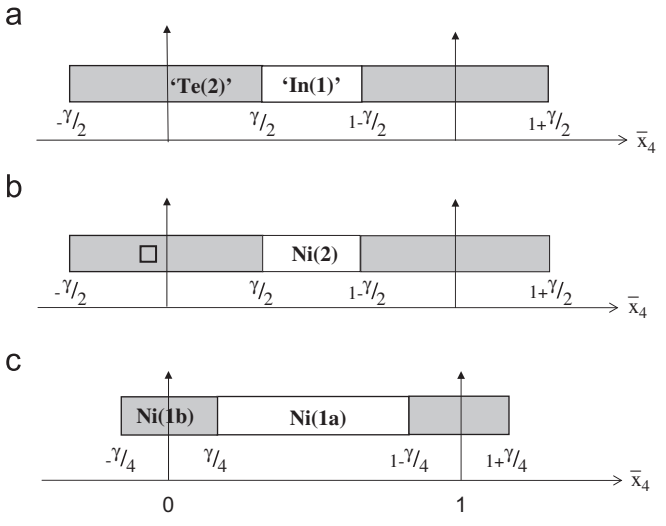

Fig. 6. Skis of the occupational crenel functions for the incommensurate description of ~Ni_3InTe_2 indicating the atomic domains in grey and white: (a) shows the atomic domains for the Te-rich and the In-rich layers, (b) shows the atomic domain for the Ni(2) atom in the trigonal bipyramid while (c) shows the atomic domains for fully occupied Ni(1a) and partially occupied Ni(1b) Ni octahedral sites.

tied together, e.g. if the overall B layer composition is '$In'_{1-\gamma}$'Te'_{γ}, then the width of the 'Te' occupancy domain, Δ^{Te}, must have a width in $\bar{x}_4$ of γ while the complementary width of the 'In' occupancy domain, Δ^{In}, must be $(1-\gamma)$, etc.

The observed layer stacking sequence 'Te'/'In'/'Te'/'Te'/'In'/'Te' in the case of $Ni_{3.32}InTe_2$, for example, is readily described by the 'In'/'Te' crenel function shown in Fig. 6a, i.e. by complementary crenel functions for 'Te' and 'In' with the widths in $\bar{x}_4$ set to $\Delta^{Te} = \gamma = 2/3$ for the Te occupancy domain and $\Delta^{In} = (1-\gamma) = 1/3$ for the In occupancy domain (see Fig. 6a). (From Fig. 4, for example, the parent **c** fractional co-ordinate of the six successive B type layers per superstructure repeat are given by 1/4, 3/4, 5/4, 7/4, 9/4 and 11/4, respectively, so that $\bar{x}_4 = \mathbf{q}(\mathbf{r}_\mu + \mathbf{t}) = \gamma/4$, $3\gamma/4$, $5\gamma/4$, $7\gamma/4$, $9\gamma/4$ and $11\gamma/4$ (or 1/6, 3/6, 5/6, 7/6, 9/6 and 11/6, for $\gamma = 2/3$) for these six successive B type layers. Substitution of the latter $\bar{x}_4$ values onto Fig. 6a then reproduces the observed 'Te'/'In'/'Te'/'Te'/'In'/'Te' layer stacking sequence. The same is true for the $Ni_{3.12}In_{0.86}Te_{2.14}$ sample. The only difference here is that 'In' = (0.86 In + 0.14 Te) rather than just (1.0 In + 0.0 Te) as in the case of $Ni_{3.32}InTe_2$. The apparent 'independence' of γ from the exact Te/In ratio over a limited range of Te/In values can thus be readily explained in terms of a limited solubility of In within the Te layers and/or vice versa. Provided this is taken into account, the resultant '$In'_{1-\gamma}$'Te'_{γ} composition as a function of γ implied by the occupational crenel function shown in Fig. 6a is entirely compatible with the experimentally observed composition versus wave-vector behaviour.

Likewise, the … vacant, vacant, partially occupied … stacking sequence of the trigonal bipyramidal Ni(2) layers in the case of the $Ni_{3.12}In_{0.86}Te_{2.14}$ and $Ni_{3.32}InTe_2$ samples can be described with exactly the same shape for its occupational crenel function, i.e. a single crenel function with an occupancy domain width of $\Delta^{vacancy} = \gamma = 2/3$ for the vacancy occupancy domain and $\Delta^{Ni(2)} = \Delta^{In} = (1-\gamma) = 1/3$ for the occupied layers (see Fig. 6b). The occupied trigonal bipyramidal sites can then occur only within an 'In' layer as would be expected on crystal chemical grounds given the need to match the a axis dimension of the Ni(2)/'In' layers with that of the 'Te' layers. Note further that the experimentally observed range of γ, $2/3 \leqslant \gamma \leqslant 1$, ensures that 'In' layers can never neighbour one another. The real space effect of these two occupational crenel functions for the case $\gamma = 2/3$ is shown in the inner crenel-like, occupational bar diagram shown on the left hand side of Fig. 4 where the Te layers always occur only within the grey shaded regions, of c parent unit cell length $\delta^{Te} = 1/\gamma \times \Delta^{Te} = 1/\gamma \times \gamma = 1$, whereas the In and trigonal bipyramidal Ni(2) layers always occur only within the unshaded white regions of length $\delta^{In,Ni(2)} = 1/\gamma \times \Delta^{In,Ni(2)} = 1/\gamma(1-\gamma) = 1/2$ for $\gamma = 2/3$ (reducing to 0 for $\gamma = 1$).

The only possible choice for the octahedral Ni(1a)/Ni(1b) crenel function is that shown in Fig. 6c given the above end-member commensurate superstructure refinements (for $\gamma = 2/3$) coupled with the requirement that the occupational crenel functions in Fig. 6 must give rise to the end-member $Ni_{1+y}Te_2$ structure of CdI_2 structure type for $\gamma = 1$. It is also entirely compatible with the experimentally observed relationship between Ni content and γ (see Fig. 3b). The real space effect of this Ni(1a)/Ni(1b) occupational crenel function (for the $\gamma = 2/3$ case) is shown in the second crenel-like, bar diagram on the furthest left hand side of Fig. 3. Note that the partially occupied Ni(1b) layers always occur within the unshaded white regions, of c parent unit cell length $\delta^{Ni(1b)} = 1/\gamma \times \Delta^{Ni(1b)} = (1/\gamma) \times (\gamma/2) = 1/2$, whereas the fully occupied Ni(1a) layers always occur only within the larger striped regions, of length $\delta^{Ni(1a)} = (1/\gamma) \times \Delta^{Ni(1a)} = (1/\gamma) \times (1-\gamma/2) = 1$ for $\gamma = 2/3$ (reducing to 1/2 for $\gamma = 1$).

With the use of the three occupational crenel functions shown in Fig. 6, both the formal overall stoichiometry, $Ni_{1-\gamma/2(1-occ[Ni(1b)])+occ[Ni(2)](1-\gamma)}$'$In'_{1-\gamma}$'$Te'_{\gamma}$, as well as the coupled 'In'/'Te' and Ni/vacancy ordering for any magnitude of wave vector γ can then be straightforwardly written down. In the case of $\gamma = 5/7$, for example, the predicted 'In'/'Te' layer stacking sequence is Te-Te-Te-Te-In-Te-Te-In-Te-Te-In-Te-Te-In-Te while, for $\gamma = 3/4$, the predicted 'In'/'Te' layer stacking sequence is Te-Te-In-Te-Te-Te-Te-In-Te, etc. Note that the 'In' layers always remain isolated and that their frequency of occurrence diminishes rapidly as γ increases. Note also that the number of consecutive 'Te' layers in a superstructure repeat distance is always two times an integer = 2, 4, 6, etc. and that the occurrence of the larger block sizes increases as γ increases. Finally, note that the Ni(1b) occupational domain width of $\gamma/2$ ensures that the Ni(1b) and Ni(1a) layers between neighbouring Te sheets must always alternate between partially occupied and fully occupied thus generating a slab of ideal CdI_2 structure type (cf. Fig. 1c). In the formal limit of $\gamma = 1/1$, the crenel functions of Fig. 6 thus automatically generate the $Ni_{1+y}Te_2$ structure of CdI_2 structure type as required.

Having described the occupational modulation functions associated with a general modulation wave vector, it remains to take into account the associated displacive modulations. Given the ~0.051 Å shift of the Ni(2) atoms away from the In layers and the ~0.069 Å shift of the Te layers away from the Ni(1) layers in the case of the refined structure of $Ni_{3.32}InTe_2$ given above, it is clear that displacive modulations also need to be included for a complete incommensurate structure refinement. Additional sinusoidal displacive modulation waves describing these displacive shifts were thus included.

Structure refinements of $Ni_{3.32}InTe_2$ and $Ni_{3.12}In_{0.86}Te_{2.14}$ in the commensurately modulated approach then converged smoothly. The global phase value used was $\phi = 1/2$ corresponding to space group symmetry $P6_3/mmc$. In the case of $Ni_{3.32}InTe_2$ at 10 K, the refinement statistics were $R_{wp} = 4.81\%$ for seven refined structural parameters. The $Ni_{3.12}In_{0.86}Te_{2.14}$ structure was also successfully refined in the same manner.

3.3.2.2. Ni_3InTe_2 ($\gamma = 0.71$). The refinement of the $P6_3/mmc$ average structure of the incommensurately modulated Ni_3InTe_2 sample was straight-forward and converged quickly to the residuals $R_w(obs) = 1.76\%$ $R_w(all) = 1.76\%$ and $R_{wp} = 5.60\%$ for 41 observed and 2 unobserved reflections. Only three atomic parameters were refined at this stage: an overall ADP and the average occupancies of the octahedral and trigonal bipyramidal Ni atom sites.

That higher order harmonic satellite reflections (up to third order) are visible in electron diffraction patterns of Ni_3InTe_2 (see e.g. Fig. 3a(ii)) suggests the appropriateness of the crenel function approach described above. The coupled In/Te and Ni/vacancy ordering of Ni_3InTe_2 were thus described using the same occupational crenel functions (as shown in Fig. 6). In the NPD data, however, the observed satellite reflections were, in general, relatively weak and mainly of first order (see Fig. 7; Table 3). A careful study of the peak shape of the first order harmonic satellite reflections indicates that they were slightly broader than the average structure reflections suggesting the presence of a small amount of microstructural stacking faulting (or phason wobbling). Such faulting would have the effect of decreasing the relative intensities of the higher order harmonic satellite reflections as well as smearing the satellite reflections out.

Refinement of the incommensurate structure using the same occupational crenel functions (as shown in Fig. 6) proceeded smoothly. In the final refined model (see Tables 4 and 5), the composition was fixed to the nominal composition by setting 'In' to $In_{0.970}Te_{0.030}$ and 'Te' to $Te_{0.928}In_{0.072}$ while SOF[Ni(1*b*)]/SOF[Ni(2)] was varied. The amplitudes of the sinusoidal displacive modulation waves along *c* on the Ni(1) and 'Te/In' sites (labelled $z\sin[Ni(1b)]$ and $z\sin['Te/In']$ in what follows) then refined to values of $z\sin[Ni(1b)] = 0.010(1)c_p = 0.052$ Å and $z\sin['Te/In'] = -0.014(2)c_p = -0.073$ Å, respectively, in good agreement with the values for the same parameters refined for $Ni_{3.12}In_{0.86}Te_{2.14}$ and $Ni_{3.32}InTe_2$. The inclusion

Table 4
Refined cell parameters from the incommensurate refinements of Ni_3InTe_2

	Sample Ni_3InTe_2	
	10 K	295 K
a	3.9901(2)	3.9989(2)
c	5.2313(3)	5.2470(3)
c/*a*	1.3111	1.3121
γ	0.7088(9)	0.7088(9)

Table 5
Refined parameters from the incommensurate refinements of Ni_3InTe_2

	Sample Ni_3InTe_2	
	10 K	295 K
U_{iso}[all]	0.0070(3)	0.0129(4)
SOF [Ni(1*a*)]	1	1
SOF [Ni(1*b*)]	0.714(6)	0.702(7)
SOF [Ni(2)]	0.373	0.371
SOF [In(1)/Te(1)]	0.970/0.030	0.970/0.030
SOF [Te(2)/In(2)]	0.928/0.072	0.928/0.072
$z\sin1$[Ni(1*a*,*b*)]	0.008(1)	0.010(1)
$z\sin1$[In/Te]	−0.011(2)	−0.014(2)

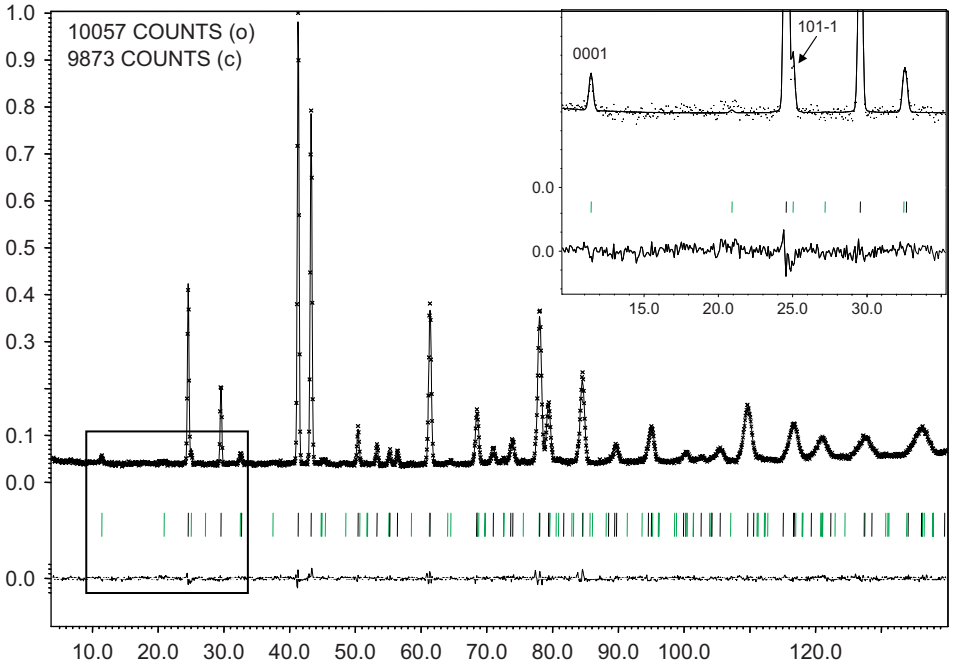

Fig. 7. The final profile fit for the sample Ni_3InTe_2 (at 10 K). The marked portion of the image is blown up in the top right corner to emphasise the fit of the satellite reflections.

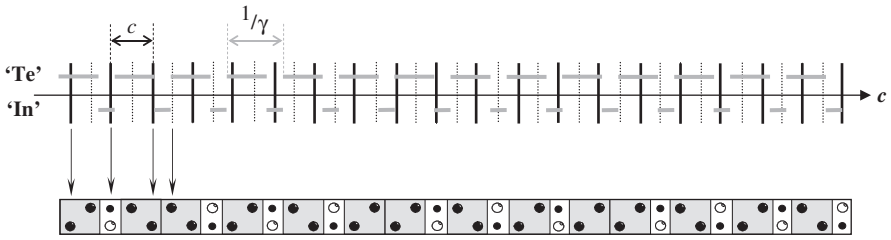

Fig. 8. An illustration of the incommensurate real-space structure of Ni_3InTe_2 built up using a crenel approach. The upper part shows the periodicity of the parent structure along the *c*-direction in real space. The bold vertical lines illustrate atomic layer lines (in this case the "anionic ones") with a spacing equal to that of the parent *c*-axis (c_p). The vertical dotted line situated halfway between, illustrate the position of the intermediate "anionic layer". The real space atomic modulation function (AMF) is illustrated in thick grey horizontal lines. The length of the function is $1/\gamma$, which is $\sim 1.41 c_p$ (see text for details). The stacking sequence of (predominately) Te layers and (predominately) In layers is given by which part of the AMF that intersects a particular "atomic layer line". The resulting structure is given in the lower part of the figure illustrated with the same building blocks as in Fig. 4.

of these displacive modulations reduced the residuals for the refinement significantly (e.g. R_{wp} reduced from 4.94% to 4.82% while R_w(all) reduced from 2.98% to 2.34% for the 10 K refinement). The final residuals for both the 10 and 295 K refinements are summarized in Table 3 and the final profile fit and difference plot is shown in Fig. 7 for the 10 K refinement while. As in total only five parameters were refined, the fit is relatively good. A portion of the final refined structure is shown in Fig. 8.

4. Discussion and conclusions

The composition range for the *NiAs/Ni₂In* type SS2 solid solution phase is considerably broader than previously reported [7] and indeed appears to connect with the CdI_2 type SS1 phase field (see Fig. 2). Commensurate superstructure as well as (3 + 1)-d incommensurate structure refinements at three separate compositions ($Ni_{3.32}InTe_2$, $Ni_{3.12}In_{0.86}Te_{2.14}$ and Ni_3InTe_2) and two primary modulation wave vector magnitudes ($\gamma = 2/3$ for $Ni_{3.32}InTe_2$ and $Ni_{3.12}In_{0.86}Te_{2.14}$ and $\gamma = 0.71$ for Ni_3InTe_2) within this extensive solid solution field show that the structure at any particular composition can be described in terms of the intergrowth of Ni_{1+y}'Te'$_2$ slabs of CdI_2 structure type intergrown with Ni_{1+y}'In' single layers of *Ni₂In* structure type. The single layer nature of the Ni_{1+y}'In' portions of the overall structure, i.e. the fact that 'In' layers are never allowed to neighbour one another, is a constraint that determines the lower bound ($\gamma = 2/3$) for the continuously variable, largely composition-determined, modulation wave vector magnitude while the formal upper bound for γ of 1 occurs at the $Ni_{1+y}Te_2$ composition of CdI_2 structure type. The reason the primary modulation wave vector magnitude γ is not precisely determined by the In/Te ratio is the small solubility of Te into the In layers and vice versa.

Recently, the crystal structures of the two compounds T_3GeTe_2 (T = Fe, Ni) were reported [17]. In the case of Fe_3GeTe_2, the structure was described as composed of layers of 'T_3Ge' sandwiched between Te-layers with a van der Waals gap between the Te layers. For the Ni-analogue phase an additional Ni atom was placed in this van der Waals gap making the Ni-analogue more closely related to the compositions studied here. The structures of $Ni_{3.32}InTe_2$ and $Ni_{3.12}In_{0.86}Te_{2.14}$ reported in this paper are clearly related, if not isomorphous, to these structures. The reported Ge/Te/Te *B* layer stacking sequence, for example, is directly isomorphous to the In/Te/Te stacking sequence found in our case. The refined occupancies of the various T metal atom sites, however, differ significantly. The occupancy of the site analogous to our Ni(1*b*) octahedral site is reported to be zero in the case of the T = Fe compound and only 0.25 in the case of the T = Ni compound while the occupancy of the trigonal bipyramidal site equivalent to our Ni(2) site, for example, is fully occupied in the case of these T_3GeTe_2 (T = Fe, Ni) compounds. The latter is likely due to a greater need to expand the Ge/T-layer in the T_3GeTe_2 compounds in order to make them fit to the Te-layers, In atoms being significantly larger than Ge. It would be intriguing to know whether there is any evidence for solid solution behaviour in these Fe–Ge–Te and Ni–Ge–Te systems analogous to that we have found in the Ni–In–Te system.

Acknowledgments

The authors would like to thank Mr. James Downs for his help with the synthesis of some of the samples. Financial support for the data collection (A.K.L. and L.N.) was given by the Swedish Research Council (VR). Financial support from the Australian Research Council (A.K.L. and R.L.W.) is also gratefully acknowledged.

References

[1] P. Villars, L.D. Calvert (Eds.), Pearsons Handbook of Crystallographic Data for Intermetallic Phases, ASM International, OH, 1991.
[2] T.B. Massalski (Ed.), Binary Alloy Phase Diagrams, American Society for Metals, Metals Park, OH, 1986.
[3] S. Lidin, A.-K. Larsson, J. Solid State Chem. 118 (1995) 313–322.
[4] L. Norén, R.L. Withers, Y. Tabira, J. Alloys Compds. 309 (2000) 179–187.
[5] L. Norén, A.-K. Larsson, R.L. Withers, H. Rundlöf, J. Alloys Compds. 424 (2006) 247–254.
[6] L. Norén, V. Ting, R.L. Withers, G. Van Tendeloo, J. Solid State Chem. 161 (2001) 266–273.

[7] L. Norén, R.L. Withers, F. Brink, J. Alloys Compds. 353 (2003) 133–142.
[8] K.O. Klepp, K.L. Komarek, Monatsh. Chem. 103 (1972) 934–946.
[9] S. Furuseth, K. Selte, A. Kjekshus, Acta Chem. Scand. 19 (1965) 257–258.
[10] T. Janssen, A. Janner, A. Looijenga-Vos, P.M. de Wolff, Incommensurate and commensurate modulated structures, in: A.J.C. Wilson (Ed.), International Tables for Crystallography, vol. C, Kluwer Academic Publishers, Dordrecht, 1995, pp. 797–835.
[11] J.M. Pérez-Mato, in: J.M. Pérez-Mato, F.J. Zuniga, G. Madariaga (Eds.), Methods of Structural Analysis of Modulated Structures and Quasicrystals, World Scientific, 1991, pp. 117–218.
[12] P.M. de Wolff, Acta Crystallogr. A 30 (1974) 777–785.
[13] V. Petříček, M. Dušek, L. Palatinus, JANA2000, Institute of Physics, Praha, Czech Republic, 2000.
[14] O. Gourdon, V. Petříček, M. Dušek, P. Bedzicka, S. Durovic, D. Gyespesova, M. Evain, Acta Crystallogr. B 55 (1999) 841–848.
[15] L. Elcoro, J.M. Perez-Mato, R.L. Withers, Z. Krist. 215 (2000) 727–739.
[16] J.M. Perez-Mato, M. Zakhour, F. Weill, J. Darriet, J. Mater. Chem. 9 (1999) 2795–2808.
[17] H.-J. Deiseroth, K. Aleksandrov, C. Reiner, L. Kienle, R.K. Kremer, Eur. J. Inorg. Chem. 8 (2006) 1561–1567.